

UC Office of the President

Recent Work

Title

Laser driven electron acceleration in nanorod arrays targets

Permalink

<https://escholarship.org/uc/item/0mz7q1ws>

Authors

Knyazev, A R
Zhang, Y
Krasheninnikov, S I

Publication Date

2020

Peer reviewed

Laser driven electron acceleration in nanorod arrays targets

A. R. Knyazev, Y. Zhang and S. I. Krasheninnikov¹

University California San Diego, La Jolla, CA 92093-0411,

USA

This paper describes the stochastic electron acceleration of the electrons by the high-intensity laser in the presence of the quasi-static fields, created from the interaction of the laser with the nanoscale grating target. The semi-analytical model describing the formation of the quasi-static fields created during laser-target interaction is presented. The mechanism of the stochastic electron acceleration is described using the 3/2-Hamiltonian approach. The electron energy scaling with the laser and target parameters are obtained. The analysis is verified with a series of 2-dimensional particle-in-cell simulations.

I. INTRODUCTION

Interaction of high-intensity lasers with solid targets can result in high yield of both x-ray and energetic electrons. To efficiently convert the energy of the incident laser into the energy of the radiated x-ray and emitted electrons, it is necessary that the target absorbs most of the incident laser energy. Multiple studies (see^{1,2} and others) indicate that flat targets typically absorb $< 10\%$ of the laser pulse energy, while structured targets can absorb $> 90\%$. Therefore, structured targets have been regarded as a potentially efficient source of x-ray and energetic electrons. Laser interaction with different structured targets, such as nanorod arrays,^{2,3,4} "velvet" targets⁵, "smoked" targets⁶, "foamed" targets⁷, were studied experimentally and via computer simulations. However, the physics of the electron acceleration during the laser-target interaction is not yet completely described. It was reported⁸ that the interaction of the micro-channel target with the laser creates the quasistatic electric fields in the cavities of the target. Presence of static electric and magnetic field can lead to the stochastic acceleration of the electrons by the laser, as was demonstrated in^{9,10,11} with the 3/2-Hamiltonian formalism.

In this paper, we model the interaction of a laser with a periodic nanorod array target. We show that quasistatic electric and magnetic fields can emerge in such setup, and develop a semi-analytic model for the formation of such fields. We then use the 3/2-Hamiltonian approach to show that formed quasistatic fields enable the mechanism of stochastic electron acceleration and derive the corresponding maximum electron energy \mathcal{E}_{\max} . We present the scalings of \mathcal{E}_{\max} with laser amplitude and target parameters. We verify the analytic results with a series of 2-dimensional Particle-In-Cell (2D PIC) simulations. The maximum electron energy in our PIC simulations can be explained with the proposed stochastic acceleration mechanism.

The rest of the paper is organized as follows. In Section II we describe the simulation setup, introduce the notations and unit normalization used in the rest of the paper. In section III we describe the extraction of the electrons from the target by the laser pulse and the formation of quasistatic electromagnetic fields during the laser-target interaction. In section IV we present our study of the acceleration of the electron interacting with the laser and the electrostatic fields described in Section III. We present the results of our PIC simulations in Section V. Section VI is the conclusion.

II. SETUP DESCRIPTION

Laser-target interaction experiments typically involve complex, often irregular structures. Direct simulation of such structures requires a 3D consideration,^{7, 12} which poses significant computational challenges. Modeling complex structures can also make it hard to pinpoint important physics mechanisms. In this work, we consider a simplified 2D model of a nanorod target, similar to the setup in the papers.^{2, 4} Specifically, we model the target by filling a region of the simulation domain with the cold plasma, as shown with black color in Figure (1). The nanorods are modeled as rectangular regions with lengths of sides $d = 0.1\lambda$ and $L = 20\lambda$, where λ is the wavelength of the incident laser pulse in our simulations. The backplate of the target is modeled as a slab of size $L_{\text{bp}} = \lambda$. The gaps between neighboring nanorods are all equal to D , with the value of D ranging from 0.25λ to 8λ in our PIC simulations. The material of a target is modeled by a cold plasma, composed of immobile ions preionized to $Z = 5$, and the electrons. The number density of the electrons is set to $n_e = 50n_{\text{cr}}$, where $n_{\text{cr}} = m\omega^2/4\pi e^2 = 6.97 \times 10^{21} \text{ cm}^{-3}$, m is the electron mass, $\omega = 2\pi c/\lambda$ is the laser frequency. The number density of ions is set to $n_i = n_e/Z$.

In the rest of the paper, we will use the Cartesian coordinates introduced in Figure (1). We choose the reference frame so that the laser prepulse reaches the nanorods at $z = 0$ at time $t = 0$. We denote unit vectors along the coordinate axis as \mathbf{e}_x , \mathbf{e}_y and \mathbf{e}_z .

The laser is simulated as a linearly polarized plane wave pulse propagating along the z -axis, from the left boundary of the simulation domain. The wavelength of the laser is $\lambda = 400 \text{ nm}$. The polarization of the pulse is set to be either along the x -axis (x-polarized pulse), or along the y -axis (y-polarized pulse). The intensity of the laser pulse is $I = 5 \times 10^{19} \text{ W/cm}^2$, which corresponds to the normalized vector potential $a_0 = eE_{\text{max}}/m_e c\omega = 2.4$. The pulse is 19λ long, with a 2λ prepulse, 17λ main pulse and 2λ decay. The normalized vector potential of the laser pulse is therefor equal to $a = a_0 F(\xi) \sin(\xi)$, where

$$F(\xi) = \begin{cases} 0 & \text{for } \xi < 0 \text{ and } \xi > 34\pi T \\ \sin(\frac{\xi}{8T}), & \text{for } \xi \text{ from } 0 \text{ to } 4\pi T \\ 1, & \text{for } \xi \text{ from } 4\pi T \text{ to } 30\pi T \\ \sin(\frac{\xi-30\pi T}{8T}), & \text{for } \xi \text{ from } 30\pi T \text{ to } 34\pi T \end{cases}, \quad \xi = \frac{2\pi}{c}(z - ct). \quad (1)$$

The shape of the laser pulse is schematically shown on the Figure (1).

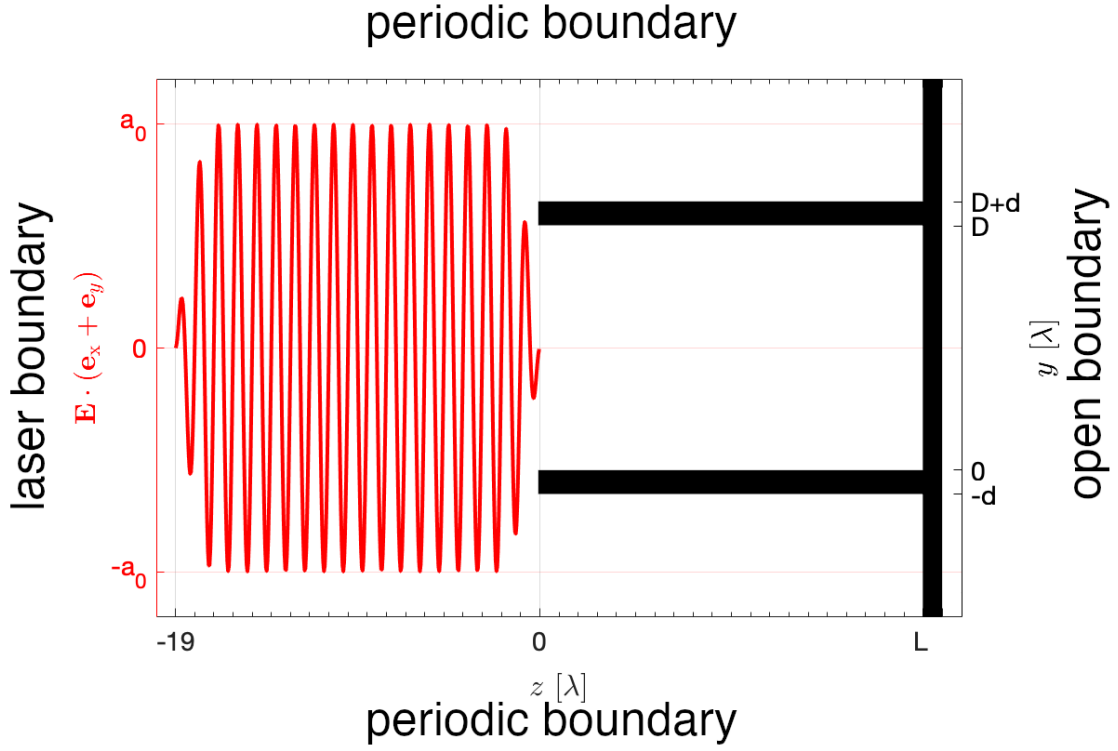


FIG. 1. Schematic view of the simulation setup. The black region corresponds to where the target is located in the domain. The nanorods are separated by an empty gap of width D . Each nanorod has the width d along y -axis and length L along z -axis. Slabs are connected on the right side with the bulk of width λ . Top and bottom boundaries of the simulation domain are periodic, left and right boundaries are open. The laser pulse arrives from the left boundary. Electric field of the laser at time $t = 0$ is shown by the red curve.

We conduct our particle-in-cell simulations with the fully relativistic 2D3V PIC code EPOCH.¹³ The simulation domain has the size of $2d + 2D$ along the x -axis, and 50λ along the y -axis. Each cell has a size of 0.01λ along both x and y axes. Boundaries normal to the y axis are periodic for both particles and fields. Boundaries normal to the z axis are open for both particles and fields.

The rest of this paper uses normalized units described in this paragraph. To indicate that the variable is normalized, its symbol is marked with a caret. Distances are normalized by $\lambda/2\pi$. Velocities of electrons \hat{v} are normalized by the speed of light c . Number densities are normalized by n_{cr} . The time \hat{t} is normalized by $1/\omega$. Momentum of electrons \hat{p} is normalized

by mc . The magnitudes of the electric $\hat{\mathbf{E}}$ and magnetic $\hat{\mathbf{B}}$ fields are normalized by $mc\omega/e$.

A. Role of the laser polarization

Polarization of the laser pulse significantly affects the laser-target interaction. Firstly, the laser pulse polarized along y axis can propagate into the gap of any size \hat{D} , while the pulse polarized along x is reflected if $\hat{D} < \pi$. Secondly, as will be discussed further in Section III, only the y -polarization pulse creates the quasistatic fields inside the gap. The difference between x and y polarization can be explained with a simple model of a lossless multi-connected waveguide (see §91 in¹⁴ for details). Specifically, consider the waveguide formed by two parallel, ideally conducting plates located at $\hat{y} = 0$ and $\hat{y} = \hat{D}$. Such waveguide has three types of $\mathbf{E}, \mathbf{B} \propto \exp(i(\hat{z} - \hat{t}))$ modes: purely transverse (a.k.a. TEM) modes, modes with longitudinal components of the electric field (a.k.a. TM modes), and modes with longitudinal components of magnetic field (a.k.a. TE modes). Note that due to $E_x = 0$ boundary conditions, TEM modes in such a waveguide can only be polarized along \mathbf{e}_y , and have the same electric and magnetic fields as a plane wave. Furthermore, TEM modes can propagate in a gap of any size \hat{D} , and have luminal phase velocity. It can explain why in our PIC simulations with the y -polarized laser pulse, the laser pulse was able to penetrate in the gap of any size \hat{D} , and the field of the pulse in the gap was the same as the y -polarized plane wave. The electric field of such TEM mode is normal to the waveguide boundary, and therefore it can extract the electrons by the electric force. Meanwhile, the only x -polarized modes in the aforementioned waveguide are TE modes. As a crude model for the propagation of the x -polarized pulse inside the gap, one can simply Fourier expand the plane wave at the gap entrance $|\mathbf{E}| = |E(y, z = 0)\mathbf{e}_x| = \tilde{E}_x = \text{const}$ into a sum of TE modes. The resulting expansion of \tilde{E}_x gives $E_{\text{TE}} = \alpha_l E_{x,l}$, where

$$\alpha_l = \frac{2\tilde{E}_x(1 - \cos(\pi l))}{\pi l}, \quad E_{x,l} \propto \sin\left(\pi l \frac{y}{D}\right), \quad l \text{ is integer.} \quad (2)$$

The expression for the z -component of magnetic field B_{TE} is $B_{\text{TE}} = \alpha_l B_{z,l}$, where $B_{z,l}$ is the z -component of magnetic field of the TE mode with electric field $E_{x,l}\mathbf{e}_x$. Electrons subjected to $E_{\text{TE}}\mathbf{e}_x$ and $B_{\text{TE}}\mathbf{e}_z$ experience ponderomotive force which expels these electrons from the gap. Therefore, any electron number density in the gap will be suppressed. Since this paper focuses on laser driven electron acceleration, in the rest of the paper we will primarily study

the case of the y-polarization.

III. ELECTRON EXTRACTION AND FORMATION OF QUASISTATIC ELECTROMAGNETIC FIELD

As the y-polarized pulse propagates between the nanorods, it extracts some of the electrons from them. The extracted electrons can then either return to their parent nanorod or stream away from it. The counterpropagating bunches of streaming electrons, extracted from the opposite boundaries of the gap between nanorods, pass through each other, mix up and form an electron gas of homogeneous density \bar{n} in the gap.

To have some understanding of extraction process we consider the following model. We consider the electron located at the boundary between the nanorod and the gap. We also assume that the field acting on this electron is the same as the field of a plane wave, propagating along the surface of the nanorod. Specifically, we consider a motion of single electron in the plane wave described by a vector potential $\mathbf{a}_p = a_0 \cos(\xi + \xi_0)\mathbf{e}_y$, where ξ_0 is the phase of the plane wave at the moment of electron extraction. The electron is assumed to be initially immobile. The motion of an initially immobile electron in a plane EM wave has three well-known integrals of motion:

$$\hat{p}_x = 0, \quad \hat{p}_y - a_0 \cos(\xi + \xi_0) = -a_0 \cos(\xi_0), \quad \gamma - \hat{p}_z = 1, \quad (3)$$

where $\gamma^2 = 1 + \hat{\mathbf{p}}^2$. Without loss of generality we set the y-coordinate of the nanorod surface from which the electron is extracted to $\hat{y}_0 = 0$. From Equations (3), it follows that

$$\frac{d\hat{y}}{d\xi} = a_0 (\cos(\xi_0) - \cos(\xi + \xi_0)). \quad (4)$$

Equation (4) shows that only specific values of the initial phase ξ_0 lead to the extraction of the electron into the gap. Indeed, if the gap is in the $\hat{y} < 0$ region, the electron is only extracted if $\sin(\xi_0) < 0$. Likewise, for the gap in $\hat{y} > 0$ region, the electron is extracted if $\sin(\xi_0) > 0$. From Equations (3) we can derive the equations for electron's trajectory,

$$\begin{aligned} \hat{y} &= a_0 (\xi \cos(\xi_0) + \sin(\xi_0) - \sin(\xi + \xi_0)), \quad (5) \\ \hat{z} - \hat{z}_0 &= \frac{a_0^2}{2} \left[\xi \left(1 + \frac{1}{2} \cos(2\xi_0) \right) + \frac{1}{4} \sin(2(\xi + \xi_0)) + 2 \sin(\xi + \xi_0) \cos(\xi_0) + \frac{3}{4} \sin(2\xi_0) \right], \quad (6) \end{aligned}$$

where z_0 is the z-coordinate of the electron before the extraction. From Equations (5) we conclude that depending on the phase ξ_0 the extracted electron may either return to its

parent nanorod or stream away from it. From Equations (5) and (6), we can estimate the maximum angle θ between the radius vector of the electron and the $y = 0$ boundary as

$$\lim_{\xi \rightarrow \infty} \frac{\hat{y}(\xi)}{\hat{z}(\xi) - \hat{z}_0} = \frac{4 \cos(\xi_0)}{a(2 + \cos(2\xi_0))} < \frac{\sqrt{2}}{a} = \tan(\theta). \quad (7)$$

The estimate given by Equation (7) neglects the effect of the Coulomb forces between the extracted electrons and the parent nanorod, and therefor is only accurate for extracted electrons with small \hat{y} . As extracted electrons move away from the parent nanorod, the value of streaming angle θ becomes less than predicted by Equation (7).

As bunches of the electrons propagate away from their parent nanorods along the y -axis, they eventually meet a bunch of counterpropagating electrons. From Equation (7), we conclude that the length L of the gap needs to be at least $L > \sqrt{2}D/a$ for the first extracted bunches of electrons to get to the center of the gap and start mixing with the counterpropagating bunches. When the mixing occurs, mixed electron bunches form the electron gas of homogeneous density \bar{n} inside the gap. The charge density $e\bar{n}$ inside the gap creates the electric field \mathbf{E}_s . The current of the extracted electrons in the gap $j = \bar{n}e\hat{v}_z$ creates the magnetic field \mathbf{B}_s . Since $\hat{v}_z < 1$, the magnitude of the magnetic field (B_s) is weaker than the magnitude of the electric field (E_s).

Assuming the electron extraction stops when the electric field \mathbf{E}_s from the electron gas compensates the electric field of the laser pulse at the boundary, the density of the electron gas can be estimated as

$$\bar{n} = \frac{2a_0}{\hat{D}}. \quad (8)$$

Concluding this section, we note the differences of the quasistatic electric and magnetic fields in the gap from the quasistatic fields in another laser-plasma interaction setup, the evacuated ion channel¹⁵. Specifically, fields associated with the electron gas create the $\mathbf{E} \times \mathbf{B}$ force along the direction of laser propagation, whereas, in the ion channel, the $\mathbf{E} \times \mathbf{B}$ force is directed against laser propagation.

IV. STOCHASTIC ACCELERATION IN QUASISTATIC POTENTIAL WELLS

The scalar $U(\hat{y})$ and vector $A_B(\hat{y})\mathbf{e}_z$ potentials, corresponding to electric $\mathbf{E}_s = (dU(\hat{y})/d\hat{y})\mathbf{e}_y$ and magnetic $\mathbf{B}_s = (dA_B(\hat{y})/d\hat{y})\mathbf{e}_x$ fields described in Section III, can be approximated with

periodic series of quadratic potential wells as

$$U(\hat{y}) = \frac{\kappa_U}{2} \left(\frac{\hat{D}^2}{4} - \left(\hat{y} - \frac{\hat{D}}{2} \right)^2 \right), \quad (9)$$

$$A_B(\hat{y}) = \frac{\kappa_B}{2} \left(\frac{\hat{D}^2}{4} - \left(\hat{y} - \frac{\hat{D}}{2} \right)^2 \right), \quad (10)$$

where $\kappa_U = \bar{n}$ and κ_B is taken smaller than κ_U , because in Section III the magnitude of static magnetic field $|\mathbf{B}_s|$ is predicted to be smaller than the magnitude of electric field $|\mathbf{E}_s|$. We note that Equations (9) and (10) neglect the size of the nanorods \hat{d} , so $\hat{d} = 0$ is assumed in this section. The presence of $U(\hat{y})$ and $A_B(\hat{y})$ potential wells alongside with the laser pulse can enable the mechanism of stochastic electron acceleration. To illustrate this acceleration mechanism, we employ the 3/2-dimensional Hamiltonian framework.^{9,10,11} The motion of a single electron in the potential wells $U(\hat{y})$ and $A_B(\hat{y})$ and the laser wave with vector potential $\mathbf{a} = a_0 \cos(\xi) \mathbf{e}_y$, can be described with the Hamiltonian formalism as

$$\frac{d\hat{P}_y}{d\xi} = -\frac{\partial H}{\partial \hat{y}}, \quad \frac{d\hat{y}}{d\xi} = \frac{\partial H}{\partial \hat{P}_y}, \quad (11)$$

where $\hat{P}_y = \hat{p}_y - a_0 \cos(\xi)$ is the canonical momentum, and

$$H = \frac{1}{2} \left\{ \frac{1 + \left[\hat{P}_y + a_0 \cos(\xi) \right]^2}{C - W^{(-)}(\hat{y})} + W^{(+)}(\hat{y}) + C \right\} = \gamma + U, \quad (12)$$

$$W^{(\pm)} = U(\hat{y}) \pm A_B(\hat{y}) \quad (13)$$

$$C = \gamma + W^{(-)}(\hat{y}) - \hat{p}_x = \text{const.} \quad (14)$$

We introduce the notations $W_*^{(-)} = (\kappa_U - \kappa_B) \hat{D}^2 / 8$ and $W_*^{(+)} = (\kappa_U + \kappa_B) \hat{D}^2 / 8 \approx a_0 \hat{D} / 2$. Note that the small difference between κ_U and κ_B is important, as it can lead to a smaller electron dephasing rate $\gamma - p_z = C - W^{(-)}(y)$.

In the rest of this section, we analyze the acceleration of electrons for different values of C to find the maximum energy \mathcal{E}_{\max} that electron can achieve by stochastic acceleration. Specifically, we consider three cases: $C \gg W_*^{(-)}$, $C < W_*^{(-)}$ and $C \gtrsim W_*^{(-)}$. For each of the cases, we find the corresponding maximum energy that the electron can achieve by stochastic acceleration and compare these energies to find the \mathcal{E}_{\max} . Since we are interested in the maximum energy of the electrons, we will only consider the electrons with relativistic energies $\mathcal{E} \gg \max(a_0 \hat{D}, C, a_0^2 / C)$.

First case is $C \gg W_*^{(-)}$. If $C \gg W_*^{(-)}$, the impact of $W_*^{(-)}$ can be neglected. Therefore, electron injected from the plasma slab with the energy $\mathcal{E} < W_*^{(+)}/2$ will first oscillate in the $W^{(+)}(\hat{y})$ potential well, with the frequency of the oscillation Ω_p depending on the electron energy \mathcal{E} as $\Omega_p \sim (\mathcal{E}/C)^{1/2}/\hat{D}$. The electron can then undergo stochastic acceleration¹¹ with energy jumps of $\Delta\mathcal{E} \sim a_0\sqrt{2\mathcal{E}/C}$ between two consecutive passages through $\hat{y} = 0$. When the electron heats up to the energy $\mathcal{E} > W_*^{(+)}/2$, it can escape the potential well and switch to what we will refer to as a “passing regime”. Because of the periodicity of $W^{(+)}(\hat{y})$, the force acting on the passing electron is also periodic. The frequency of the periodic force acting on the passing electron is $\Omega_p \approx 2\pi(2\mathcal{E}/C)^{1/2}$. The resonance between Ω_p and the laser frequency can then allow for further continuous acceleration of the electron in the passing regime. The maximum energy \mathcal{E}_{\max}^p that passing electron can achieve by stochastic acceleration can be obtained from $\Delta\mathcal{E}$ and $T_p = 2\pi/\Omega_p$ by considering the threshold for the onset of stochastic motion of the electron with $\mathcal{E} > a_0\hat{D}/4 > a_0^2/C$,

$$K \approx \frac{\partial T_p}{\partial \mathcal{E}} \Delta\mathcal{E} \sim \frac{a_0\hat{D}}{2\mathcal{E}}. \quad (15)$$

Specifically, \mathcal{E}_{\max}^p corresponds to $K = 1$ in Equation (15), and is approximately equal to

$$\mathcal{E}_{\max}^p \sim a_0\hat{D}/2 = (\hat{D}C/2a_0)(a_0^2/C) = \zeta\mathcal{E}_{\text{pond}}, \quad (16)$$

where $\mathcal{E}_{\text{pond}} = a_0^2/C$ is the ponderomotive energy scaling, and $\zeta = \hat{D}C/2a_0$ is the parameter that describes the $\mathcal{E}_{\max}^p/\mathcal{E}_{\text{pond}}$ ratio. We note that for this analysis to be valid, ζ needs to be greater than 1, and therefore we assume $\zeta > 1$ throughout this section. The energy \mathcal{E}_{\max}^p is the maximum energy that electron can achieve in the case $C \gg W_*^{(-)}$.

Next possible case is $C < W_*^{(-)}$. For $C < W_*^{(-)}$, the electrons will always remain trapped. When $C \ll W_*^{(-)}$, the electron is trapped near $|y| \ll \hat{D}$. In this regime, $W^{(-)}(y) \approx \alpha y$, with $\alpha = 2W_*^{(-)}/\hat{D} = \text{const.}$ The stochastic condition $K = 1$ predicts the maximum energy

$$\mathcal{E}_{\max}^{tr} \sim (D^8 a_0^6 C^9 / (2W_*^{(-)})^8)^{1/7} = \mathcal{E}_{\text{pond}} \zeta^{8/7} (C/2W_*^{(-)})^{8/7}. \quad (17)$$

Equation (17) suggests that \mathcal{E}_{\max}^{tr} is largest at $C \approx W_*^{(-)}$, where \mathcal{E}_{\max}^{tr} is greater than \mathcal{E}_{\max}^p .

The last possible case is $C \gtrsim W_*^{(-)}$. For $C \geq W_*^{(-)}$, only the electrons with energy $2\mathcal{E} < \mathcal{E}_{\text{tr}} = W_*^{(+)} + C + 1/(C - W_*^{(-)})$ are trapped. Furthermore, the impact of the laser pulse is stronger at $C \approx W_*^{(-)}$, given that the electron will be able to reach the peak of the potential well at $\hat{y} = \hat{D}/2$. Close to $\hat{y} = \hat{D}/2$, the magnitude of the static

electric field $|\mathbf{E}_s| = |dU/dy|$ is small, which allows the electron to stay close to $y = \hat{D}/2$ for longer while having a small dephasing rate, and therefore enables the electron to exchange energy with the laser field efficiently. For $C = W_*^{(-)}$, the time and energy variation for such trapped electrons can be estimated as $T_t \sim \hat{D}(C/\mathcal{E})^{1/2}/2 = \zeta(\mathcal{E}_{\text{pond}}/\mathcal{E})^{1/2}$ and $\Delta\mathcal{E}_t \sim a_0(\hat{D}/2)^{1/2}(\mathcal{E}/C)^{1/4} = \mathcal{E}_{\text{pond}}\zeta^{1/2}(\mathcal{E}/\mathcal{E}_{\text{pond}})^{1/4}$, where we assumed $\Delta\mathcal{E}_t > \mathcal{E}_{\text{pond}}$. The maximum possible energy due to stochastic acceleration can again be estimated from the threshold of $K = 1$ to be $\mathcal{E}_{\text{max}} \sim \mathcal{E}_{\text{pond}}\zeta^{6/5} > \mathcal{E}_{\text{max}}^{tr} > \mathcal{E}_{\text{max}}^p$. We conclude that $W^{(-)}(y) \sim C$ facilitates the acceleration of the electrons. Furthermore, for $\mathcal{E}_{\text{max}} > \mathcal{E}_{\text{tr}}$ and $C \geq W_*^{(-)}$, the trapped electrons can gain enough energy to switch to the passing regime. Since that the dephasing rate at the peak of the potential wells for the passing electron is even smaller than the dephasing rate of the trapped electron near the turning point, even further acceleration of the passing electron is possible with small $C - W_*^{(-)} > 0$, though the resulting energy has the maximum value of the same order as \mathcal{E}_{max} .

From the analysis above we conclude that the maximum energy that electron can achieve by stochastic acceleration is given by

$$\mathcal{E}_{\text{max}} \sim \mathcal{E}_{\text{pond}}\zeta^{6/5} \sim a_0^{4/5}(D/2)^{6/5}C^{1/5}, \quad (18)$$

where $C \approx W_*^{(-)}$. The $W_*^{(-)} \approx 1$ allows initially immobile electrons to reach \mathcal{E}_{max} , while smaller $W_*^{(-)}$ will require the electron to be pre-accelerated in order to reach \mathcal{E}_{max} .

We note that, from $dz/d\xi = p_z/[C - W^{(-)}]$, the speed of longitudinal displacement of the electron will increase due to the impact of the residual static field and thus the length of the gap L should be large enough to have fully accelerated electrons. Another limitation of the presented analysis is that a_0 is assumed to be independent of z coordinate, while in reality, the laser amplitude will decay as more energy gets absorbed by the target.

V. SIMULATION RESULTS

This section presents the results of our PIC simulations. We begin by presenting the structure of the electric and magnetic fields inside the gap for the cases of x-polarized incident laser pulse. Specifically, we plot the components of the electric and magnetic fields from the PIC simulations with the gap size of $\hat{D} = 4\pi$, and compare these electric and magnetic fields components to the predictions of the analytical model discussed in Subsection II A. The

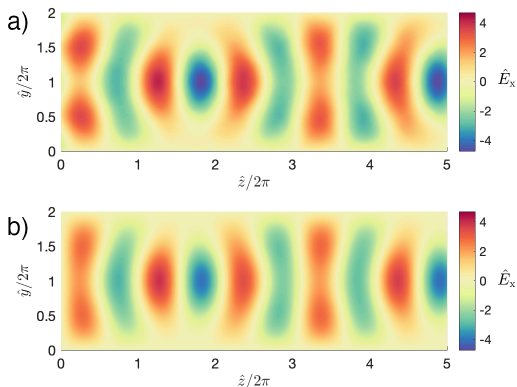


FIG. 2. The x-component of the electric field \hat{E}_x inside the gap of size $\hat{D} = 4\pi$, obtained from **a)** PIC simulation with x-polarized laser and **b)** analytical model from Subsection II A

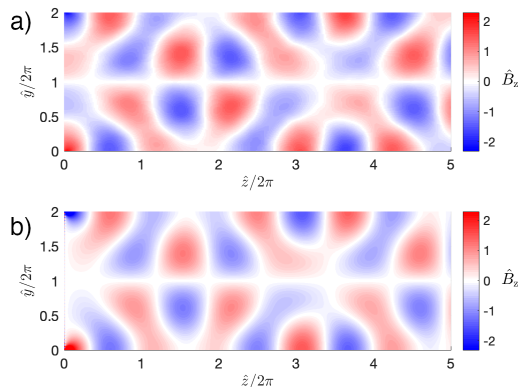


FIG. 3. The z-component of the magnetic field \hat{B}_z inside the gap of size $\hat{D} = 4\pi$, obtained from **a)** PIC simulation with x-polarized laser and **b)** analytical model from Subsection II A

x-component of the electric field \hat{E}_x from PIC simulation is shown on Figure (2(a)). The same \hat{E}_x component obtained from Equation (2) is shown on Figure (2(b)). Likewise, the z-component of the magnetic field \hat{B}_z obtained from PIC simulation with the x-polarized laser is shown on Figure (3(a)), and the same \hat{B}_z obtained from analytical model described in Subsection II A is shown on Figure (3(b)). Despite the crudeness of the analytical model presented in Subsection II A, its predictions for \hat{E}_x and \hat{B}_z match well with results of PIC simulations with x-polarized pulse.

To show how the field structure affects the electron density, we plot the electron number density \hat{n} together with electric and magnetic field components on Figures (4(a)) and (4(b)). As predicted in Subsection II A, the number density of the electrons inside the gaps is small for the case of the x-polarized incident laser.

The rest of the section shows the results of PIC simulations with the y-polarized incident laser. The electron number density \hat{n} inside the gaps of size $\hat{D} = 4\pi$ and $\hat{D} = 8\pi$ is shown on Figure (5). As predicted in Section III, the electrons extracted by the laser mix up into the electron gas of homogeneous density, creating electric and magnetic fields. Associated with these fields are electric \hat{U}_{PIC} and vector $\hat{A}_{\text{PIC}}\mathbf{e}_z$ potentials. Profiles of \hat{U}_{PIC} and \hat{A}_{PIC} from PIC simulations with different gap sizes \hat{D} are shown on Figure (6).

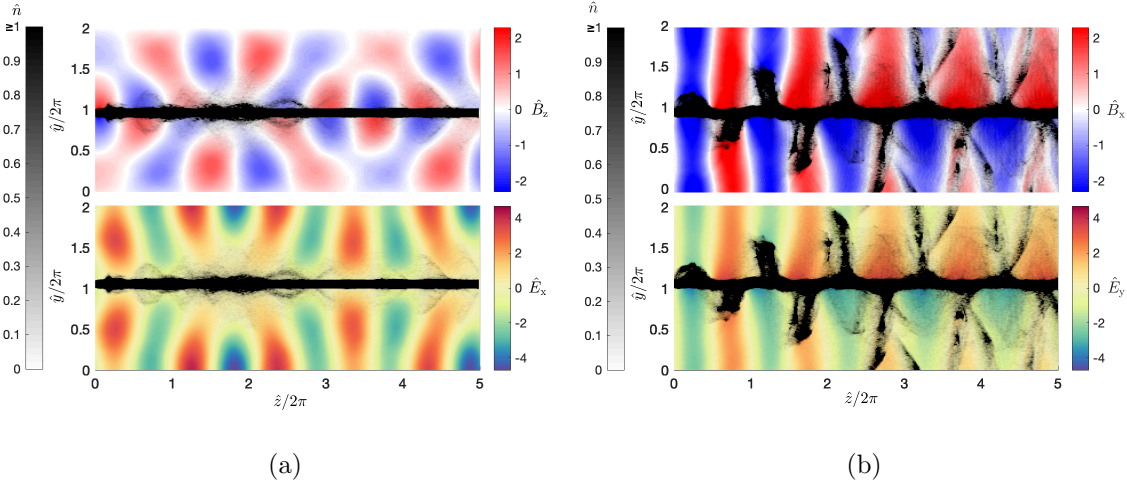


FIG. 4. Electron number density together with electric and magnetic field components from the PIC simulations with (a) x-polarized and (b) y-polarized laser pulse

Finally, we present the scaling of maximum electron energy with a_0 and \hat{D} parameters. The maximum Lorentz factor $\gamma_{\max}^{\text{PIC}}$ from simulations with different a_0 is shown on the Figure (7). Likewise, $\gamma_{\max}^{\text{PIC}}$ from simulations with different \hat{D} is shown on the Figure (8). The scaling we obtained from the PIC simulations is $\gamma_{\max}^{\text{PIC}} \propto a_0^{0.98} \hat{D}^{0.51}$, where we assumed $C \approx 1$ for all simulations. We note that increasing \hat{L} in simulations with larger \hat{D} increased the value of $\gamma_{\max}^{\text{PIC}}$, which can be explained by truncation error of PIC simulations with moderate L , as discussed in Section IV.

VI. CONCLUSION

We have examined the physics of laser driven acceleration during the interaction of a high-intensity laser with periodic nanorod array target. Specifically, we developed a quasi-analytical model of the electric and magnetic field in the gaps of the target. We showed that the structure of electric and magnetic fields inside the gap could be explained with a simple lossless waveguide theory and a single particle model of the electron extraction. We showed that if the target has dimensions $L > \sqrt{2}D/a$, then irradiating this target by a y -polarized can create a homogeneous electron gas inside the gaps of the target. We also showed that the number density \bar{n} of this homogeneous electron gas is related to the amplitude of the a_0 of the incident laser and to the gap size \hat{D} by Equation (8). We explained the difference in the magnitude of static electric and magnetic fields created by the electron gas. We then

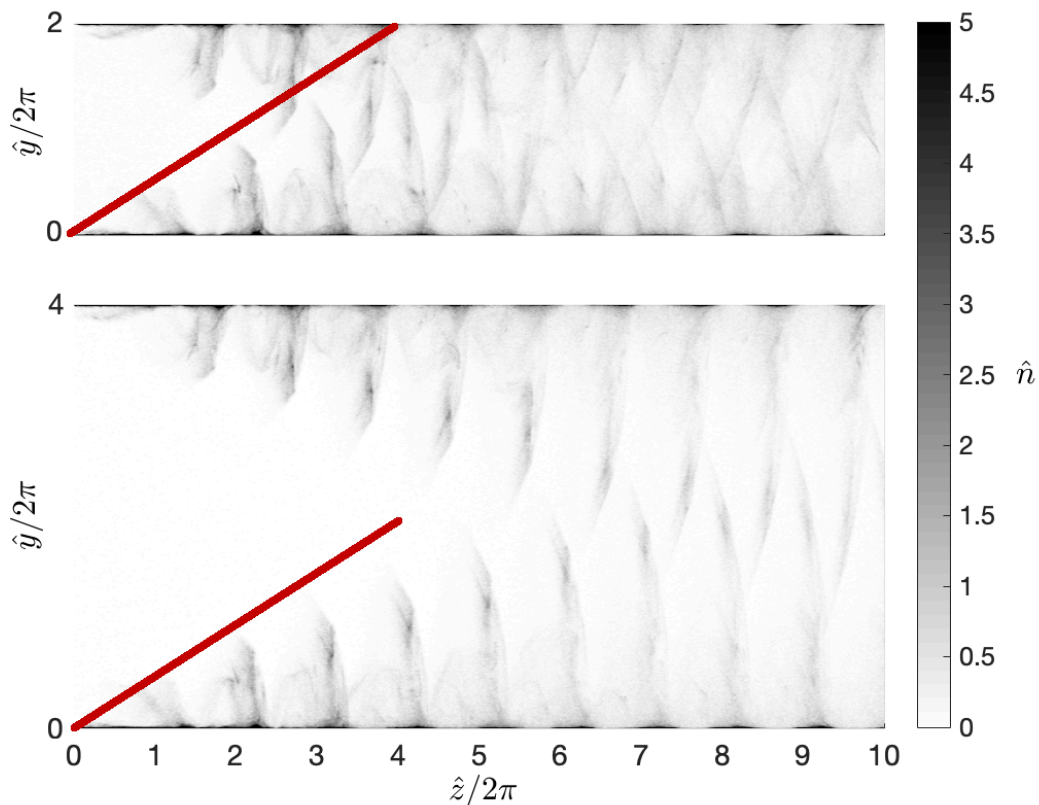


FIG. 5. Electron number density inside the gap for $\hat{D} = 4\pi$ (top) and $\hat{D} = 8\pi$ (bottom), showing the process of the electron extraction and mixing of the counterpropagating extracted electron bunches. Red lines show the maximum angle θ of extraction predicted by the single electron model in Equation (7)

described the acceleration of the electron with a laser in the presence of the aforementioned quasistatic fields using the 3/2 Hamiltonian formalism. From the 3/2-Hamiltonian model, we found the maximum energy \mathcal{E}_{\max} that the electron can achieve by stochastic acceleration. We also derived how \mathcal{E}_{\max} scales with a_0 and D . Finally, we identified the important role that the residual between quasistatic electric and magnetic field plays in stochastic acceleration. We have conducted a series of PIC simulations to verify our analysis results and found a good agreement between our semi-analytic model and numerical simulation results.

Our findings can be useful to interpret the results of the laser-target interaction studies.

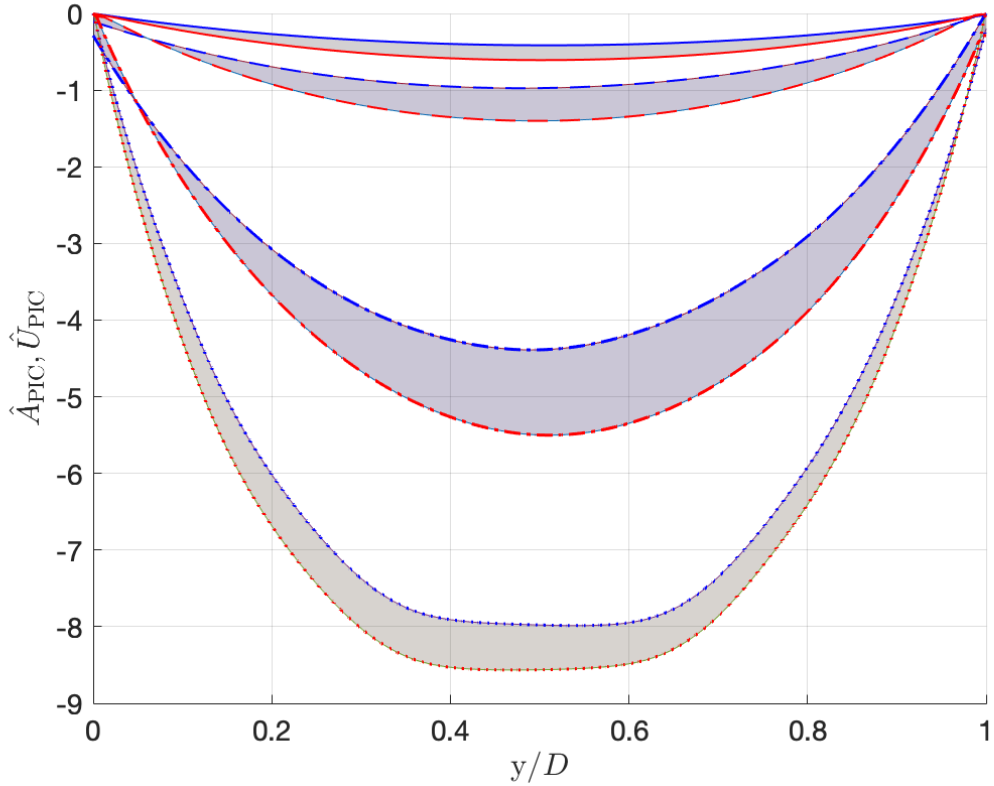


FIG. 6. Profiles of the electrostatic potential U_{PIC} (red) and vector potential $A_{\text{PIC}}\mathbf{e}_z$ (blue), describing the fields \mathbf{E}_s and \mathbf{B}_s from the PIC simulations for different values of \hat{D} . The values of \hat{D} are 0.5π (solid curves), π (dashed curves), 4π (dash-dotted curves) and 8π (dotted curves). Shaded regions correspond to the relative difference between the electric and magnetic potentials

ACKNOWLEDGMENTS

This work was supported by the University of California Office of the President Lab Fee Grant No. LFR-17-449059.

REFERENCES

- ¹M. M. Murnane and H. C. Kapteyn, “Efficient coupling of high-intensity subpicosecond laser pulses into solids,” *Appl. Phys. Lett.* 62, 1068 (1993).
- ²M. A. Purvis, et al., “Relativistic plasma nanophotonics for ultrahigh energy density physics,” .

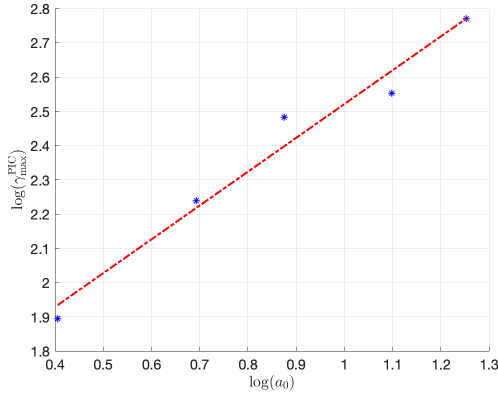


FIG. 7. Scaling of the maximum electron Lorentz factor with laser amplitude a_0 , obtained from a series of PIC simulation. Stars represent the data from PIC simulation, red line is the linear fit of the data. The slope of linear fit is 0.98, matching well with the scaling from Equation (18)

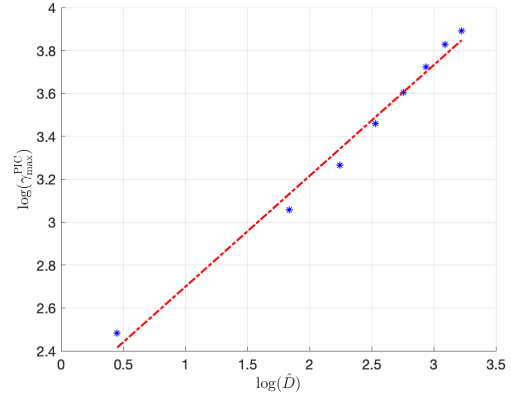


FIG. 8. Scaling of the maximum electron energy with gap size \hat{D} , obtained from a series of PIC simulation. Stars represent the data from PIC simulation, red line is the linear fit of the data. The slope of linear fit is 0.5

³A. A. Andreev et al., “X-ray generation by fast electrons propagating in nanofibres irradiated by a laser pulse of relativistic intensity,” *Quantum Electronics* vol.46 (2016).

⁴A. A. Andreev and K. Y. Platonov, “Generation, transport, and focusing of fast electrons in nanofilaments of a target irradiated by a short laser pulse with ultrarelativistic intensity,” *Quantum Electronics* vol.46 (2016).

⁵F. Y. Khattak et al., “Intense Picosecond X-Ray Pulses from Laser Plasmas by Use of Nanostructured ”Velvet” Targets,” (2000).

⁶F. Y. Khattak et al., “Enhanced He- emission from ”smoked” Ti targets irradiated with 400 nm, 45 fs laser pulses,” *Europhysics Letters*, vol. 72, (2005).

⁷L. F. et al., “Ultra-intense laser interaction with nanostructured near-critical plasmas,” *Scientific Reports* (2017).

⁸J. Snyder, et al., *Phys. of Plasmas* 26 , 033110 (2019).

⁹Y. Zhang and S. Krasheninnikov, “Electron dynamics in the laser and quasi-static electric and magnetic fields,” *Physics Letters A* **382**, 1801–1806 (2018).

- ¹⁰Y. Zhang and S. Krasheninnikov, “Electron heating in the laser and static electric and magnetic fields,” *Physics of Plasmas* **25**, 013120 (2018).
- ¹¹Y. Zhang, S. Krasheninnikov, and A. Knyazev, “Stochastic electron heating in the laser and quasi-static electric and magnetic fields,” *Physics of Plasmas* **25**, 123110 (2018).
- ¹²e. a. Clayton Bargsten, “Energy penetration into arrays of aligned nanowires irradiated with relativistic intensities: Scaling to terabar pressures,” *SCIENCE ADVANCES* (2017).
- ¹³T. D. Arber and e. a. Bennett, “Contemporary particle-in-cell approach to laser-plasma modelling,” *Plasma Physics and Controlled Fusion* **57**, 1–26 (2015).
- ¹⁴L. D. Landau, E. M. Lifshitz, “Volume 8, Electrodynamics of Continuous Media,” .
- ¹⁵A. V. Arefiev et al., “Novel aspects of direct laser acceleration of relativistic electrons,” *J. Plasma Physics* **81** (2015).